The Astrophysical Journal, 973:33 (9pp), 2024 September 20 https://doi.org/10.3847/1538-4357/ad5c3a
© 2024. The Author(s). Published by the American Astronomical Society.
OPEN ACCESS

# Filamentary Structures Formation around a Magnetic Pore Using High-resolution Observations of the Goode Solar Telescope

Jie Zhao[1], Fu Yu[1], Xiaoshuai Zhu[2], Xu Yang[3,4], Jiangtao Su[5,6], Brigitte Schmieder[7,8,9], Hui Li[1,10], and Wenda Cao[3,4]

[1] Key Laboratory of Dark Matter and Space Astronomy, Purple Mountain Observatory, Chinese Academy of Sciences, Nanjing, People's Republic of China; zhaojie@pmo.ac.cn
[2] State Key Laboratory of Space Weather, National Space Science Center, Chinese Academy of Sciences, Beijing, People's Republic of China
[3] Center for Solar-Terrestrial Research, New Jersey Institute of Technology, 323 Martin Luther King Boulevard, Newark, NJ 07102, USA
[4] Big Bear Solar Observatory, New Jersey Institute of Technology, Big Bear City, CA 92314, USA
[5] Key Laboratory of Solar Activity, National Astronomical Observatories, Chinese Academy of Sciences, Beijing 100012, People's Republic of China
[6] School of Astronomy and Space Science, University of Chinese Academy of Sciences, Beijing 101408, People's Republic of China
[7] LESIA, Observatoire de Paris, Université PSL, CNRS, Sorbonne Université, Université de Paris, 5 place Jules Janssen, 92195 Meudon, France
[8] Centre for Mathematical Plasma Astrophysics, Department of Mathematics, KU Leuven, 3001 Leuven, Belgium
[9] LSUPA, School of Physics and Astronomy, University of Glasgow, Glasgow, UK
[10] School of Astronomy and Space Science, University of Science and Technology of China, Hefei 230026, People's Republic of China
*Received 2024 April 7; revised 2024 June 6; accepted 2024 June 23; published 2024 September 13*

## Abstract

With the aid of high-resolution spatial and temporal observations from the Goode Solar Telescope, we present an investigation of the emergence, coalescence, and submergence of a moving magnetic feature (MMF) in the region surrounding a magnetic pore located at the periphery of a large sunspot. The results show that the MMF has a magnetic field strength greater than 500 G and is dominated by the horizontal magnetic component. We observe upflow at the inner part and downflow at the outer part, indicating a pattern of Evershed flow. The MMF emergence is accompanied by the expansion of a granule, which has several striations inside just like the twisted features found in the penumbra filament. Our analysis shows that although these striations have different properties of magnetic field and kinematics during the expansion of the granule, the overall magnetic and dynamic properties of the MMF remain stable. We find that the region where the MMF emerges and submerges becomes more penumbra-like, i.e., adjacent positive and negative values of elongated magnetic features that are parallel to each other, while the optical penumbra-like features are not apparent at the same time. Our work indicates that the dynamics of the MMF near the magnetic pore is important for the development of filamentary structure. The magnetic configuration produced by an MMF together with the elongation of a granule could thus be key to understand the formation of penumbra filaments.

*Unified Astronomy Thesaurus concepts:* Sunspots (1653); Solar magnetic fields (1503); Solar photosphere (1518)

*Materials only available in the online version of record: animation*

## 1. Introduction

Moving magnetic features (MMFs; Harvey & Harvey 1973), the small magnetic structures that move outward from the mature sunspot, have been discovered by Sheeley (1969). Most of the MMFs are found to originate inside the penumbra (Sainz Dalda & Martínez Pillet 2005; Deng et al. 2007; Sainz Dalda & Bellot Rubio 2008), and propagate radially to the network or plage region around the sunspot, i.e., the moat region (Harvey & Harvey 1973; Zhang et al. 2003; Li & Zhang 2013). However, MMFs streaming out from magnetic pores that never developed a penumbra have been observed in rare cases (Zuccarello et al. 2009; Li et al. 2015; Kaithakkal et al. 2017). The former are considered to contribute to the decay of the sunspot (Kubo et al. 2003; Hagenaar & Shine 2005; Deng et al. 2007; Li et al. 2019; Peng et al. 2024). The relationship between the MMF and the penumbra field has been intensively discussed. MMFs are considered to be the manifestation of serpentine field lines (Ryutova et al. 1998; Yurchyshyn et al. 2001; Zhang et al. 2003; Li et al. 2010) with an Ω shape (Schlichenmaier 2002; Weiss et al. 2004; Criscuoli et al. 2012) or a U shape (Zhang et al. 2003; Sainz Dalda & Bellot Rubio 2008; Lim et al. 2012), or a combination of uncombed field lines (Thomas et al. 2002) emanating from the sunspot. MMFs as independent structures have also been suggested (Zuccarello et al. 2009). Evershed flow is considered to play a role in driving out the MMFs (Ryutova et al. 1998; Martínez Pillet 2002; Schlichenmaier 2002; Thomas et al. 2002). According to the magnetic flux evolution of a penumbra-forming pore, the emerging flux of bipoles in between the polarities of the active region, which appears as MMFs, is considered to play an important role in supplying the magnetic flux of the penumbra, although the penumbra itself is formed near the pore at the opposite side from the emerging flux (Schlichenmaier et al. 2010a, 2010b; Rezaei et al. 2012).

In this work, an emerging flux element that appears as an MMF is identified at the boundary of the magnetic pore and shows an apparent twisting motion when moving outward. Different from observed in previous works, this MMF seems to be associated with the formation of a filamentary channel around the pore at the place of emergence, rather than being associated with the decaying of the pore. The observations are obtained by the Goode Solar Telescope (GST) with a resolution of $0\farcs1-0\farcs2$ and are listed in Section 2. We show the temporal

Original content from this work may be used under the terms of the Creative Commons Attribution 4.0 licence. Any further distribution of this work must maintain attribution to the author(s) and the title of the work, journal citation and DOI.

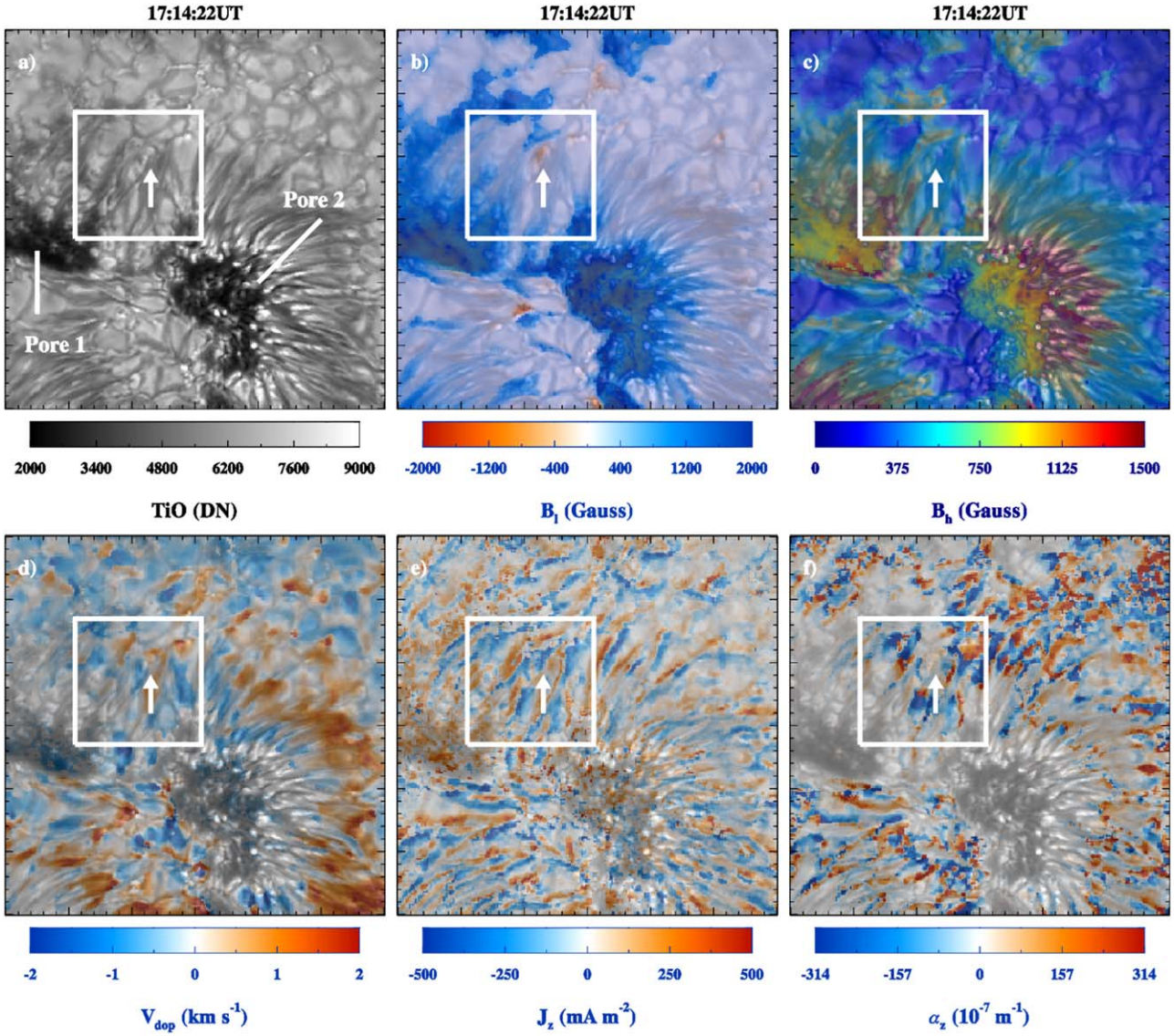


**Figure 1.** Overview of GST observations at time step 17:14:22 UT. Panels (a)–(f): the independent image of TiO and its composite images with LOS magnetic field, horizontal magnetic field, Doppler velocity, vertical current density, and local twist. The magnetic sunspots are annotated in the image of TiO with Pore 1 and Pore 2. The white square in each panel shows the ROI of the emerging flux for investigation. The animation proceeds from 17:02 to 17:44 UT in steps of approximately 1:13. The duration of the animation is 10 s.

(An animation of this figure is available in the online article.)

evolution of the MMF in Section 3 and display the detailed analysis of the fine structures in Section 4. The discussion and conclusions are presented in Section 5.

## 2. Observations

The dynamic evolution inside NOAA Active Region 12585 (N07°, W25°) has been observed in multiwavelengths with GST at the Big Bear Solar Observatory (BBSO) on 2016 September 7 from 16:24:00 UT to 18:51:00 UT. Among various emergence and submergence processes on granular scales, we investigate the one that happened inside the outskirts of a satellite sunspot—Pore 1 (see Figure 1). This work will be helpful for understanding the penumbra-filament-like structure and its fine structure whose nature has been debated until now.

The solar photosphere was observed with the Broadband Filter Imager (Cao et al. 2010) at a titanium oxide (TiO) band of 705.7 nm ($\pm$0.5 nm). The images, which have been processed with speckle reconstruction (Wöger et al. 2008), have a pixel scale of 0.″034 (Cao et al. 2010) and a temporal resolution of 30 s. The full-Stokes Near Infrared Imaging Spectropolarimeter (NIRIS; Cao et al. 2012; Ahn et al. 2016; Ahn & Cao 2019) observes the photospheric line of Fe I 1564.85 nm for magnetic Stokes profiles, with a field of view (FOV) of 58″ and a pixel scale estimated to be 0.″079 by the Scale Invariant Feature Transform algorithm (Yang et al. 2022). There are 40 spectral sampling positions from −3.16 to 3.1 Å with respect to the line center, and the cadence is around 73 s for the vector magnetic field. Parameters of magnetic field, Doppler velocity, as well as turbulence velocity, have been obtained through a Milne–Eddington inversion (such as in Wang et al. 2017), which derives comparable results with the multilayer model as shown in Yang et al. (2019). The 180° ambiguity of the azimuth angle has been resolved by the minimum-energy approach (Leka et al. 2009) for deriving the vector magnetic field. The same data set has been published in

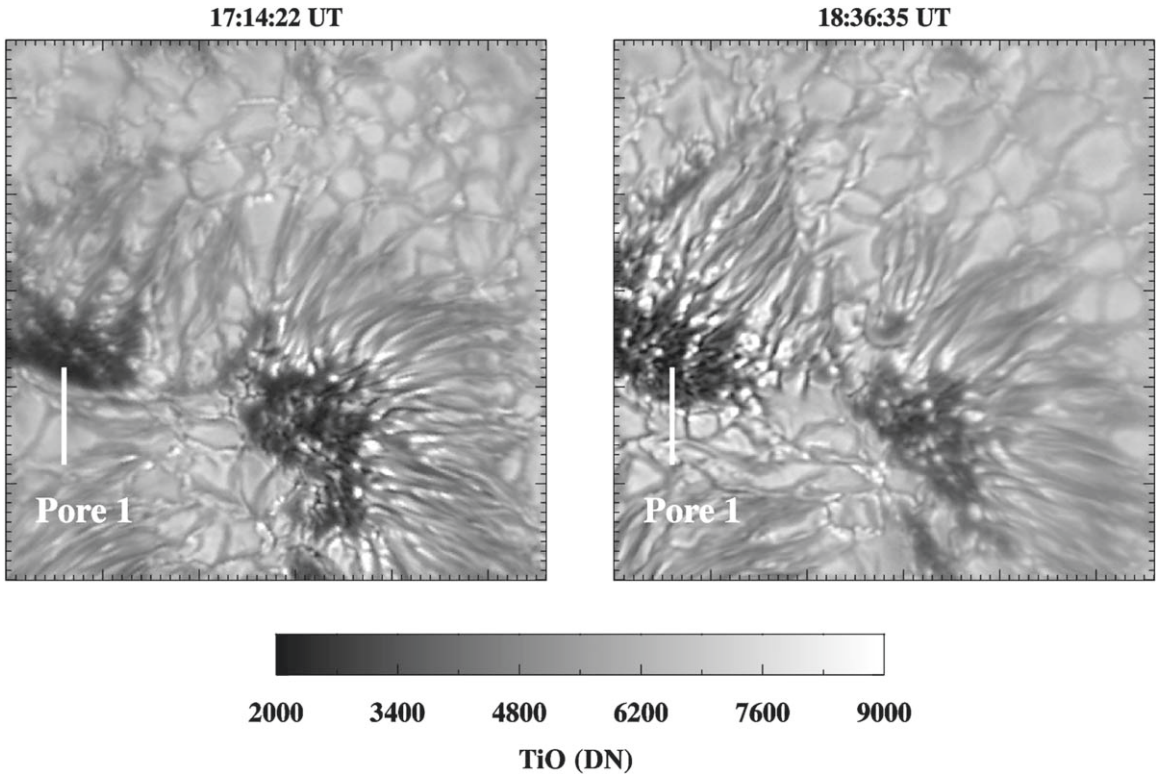


**Figure 2.** Comparison of granular structures at two time steps. The penumbra-like filamentary fibrils around Pore 1 are well pronounced at 18:36:35 UT.

Zhao et al. (2022) for the investigation of recurrent jets in between the magnetic polarities.

To better display the structures at the photosphere, the independent TiO image and its composite images overlaid with line-of-sight (LOS) magnetic field ($B_l$) and horizontal magnetic field ($B_h$) are displayed in the top row of Figure 1. The ones with Doppler velocity ($V_{dop}$), vertical current density ($J_z = (\nabla \times B)_z$), and local twist ($\alpha_z = J_z/B_z$) are displayed in the bottom row. All the images are displayed within a subregion in the FOV. The white square boxes overlaid on the images show the region of interest (ROI) of the emergence and submergence event. An animation of Figure 1 is available in the online journal.

Overall, there are two satellite pores in the subregion of the FOV. The penumbra is well developed at Pore 2, where the horizontal field is strong and the $J_z$ and $\alpha_z$ show a thin thread pattern with positive and negative values adjacent (Su et al. 2009). The Doppler velocity at the penumbra shows an upflow at the inner side and downflow at the outer side, which is a demonstration of the so-called Evershed flow (Evershed 1909) that is induced by the pressure gradient at the two footpoints of the penumbra magnetic flux tube. Although the penumbra is not well identified for Pore 1 at the time step displayed here, both the $J_z$ and $\alpha_z$ show a similar pattern in the ROI of the emerging event as in the penumbra of Pore 2 to some extent, i.e., relatively incoherent thick threads with shorter lengths. The penumbra of Pore 1 finally appears at the white box region around 18:30 UT (see Figure 2).

## 3. Temporal Evolution

The temporal evolution of the MMF is displayed in Figures 3 and 4 for the vector magnetic field, 3D dynamics, and magnetic associations, among which the surface velocity $V_{LCT}$ is obtained through local correlation tracking. The LOS magnetic field $B_l$, as well as surface velocity $V_{LCT}$ and horizontal magnetic field $B_h$ (which are displayed with arrows), are shown in the top three rows in Figure 3. Pink and green arrows show $V_{LCT}$ and $B_h$ having positive and negative LOS magnetic fields, respectively. The composite image of Doppler velocity with TiO image is shown in the fourth row and the TiO intensity is shown in the bottom row for reference. The oval in each panel shows the relevant region of the MMF. A preexisting magnetic concentration is annotated with red arrows in the left three columns except in the $V_{LCT}$ panels, and the sigmoid structure that forms during the evolution is outlined with curved lines in all panels at time steps 17:21:41 UT and 17:24:07 UT. The striations inside the MMF-associated granule are annotated with green arrows in the TiO images in the bottom row.

The MMF has a dipolar magnetic field at the initial stage. At time steps 17:04:38 UT and 17:07:04 UT, the MMF is highly sheared as seen in the distribution of the horizontal magnetic field. The expansion of the MMF-associated granule is clearly seen in the surface velocity $V_{LCT}$ and an emerging flow with a large upflow at the center is also identified in the Doppler velocity distribution. Dark fine stripes in the granule at 17:07:04 UT are found to be mainly parallel to the major axis of the granule, which is outlined by the oval.

The MMF expands continuously at time step 17:10:43 UT. It rotates (pink curved arrow) and coalesces with the preexisting magnetic concentration. The front part of the MMF (pointed to by the arrow in cyan) shows twisting motion in the $B_h$ distribution (third row), and the dark fine stripes change direction from parallel to perpendicular to the major axis of the oval. Such stripes have similar properties as the ones at time step 17:07:04 UT and the change in the morphology and location of the stripes is related to the convection flow and the expansion of the MMF. By inspecting the magnetic field

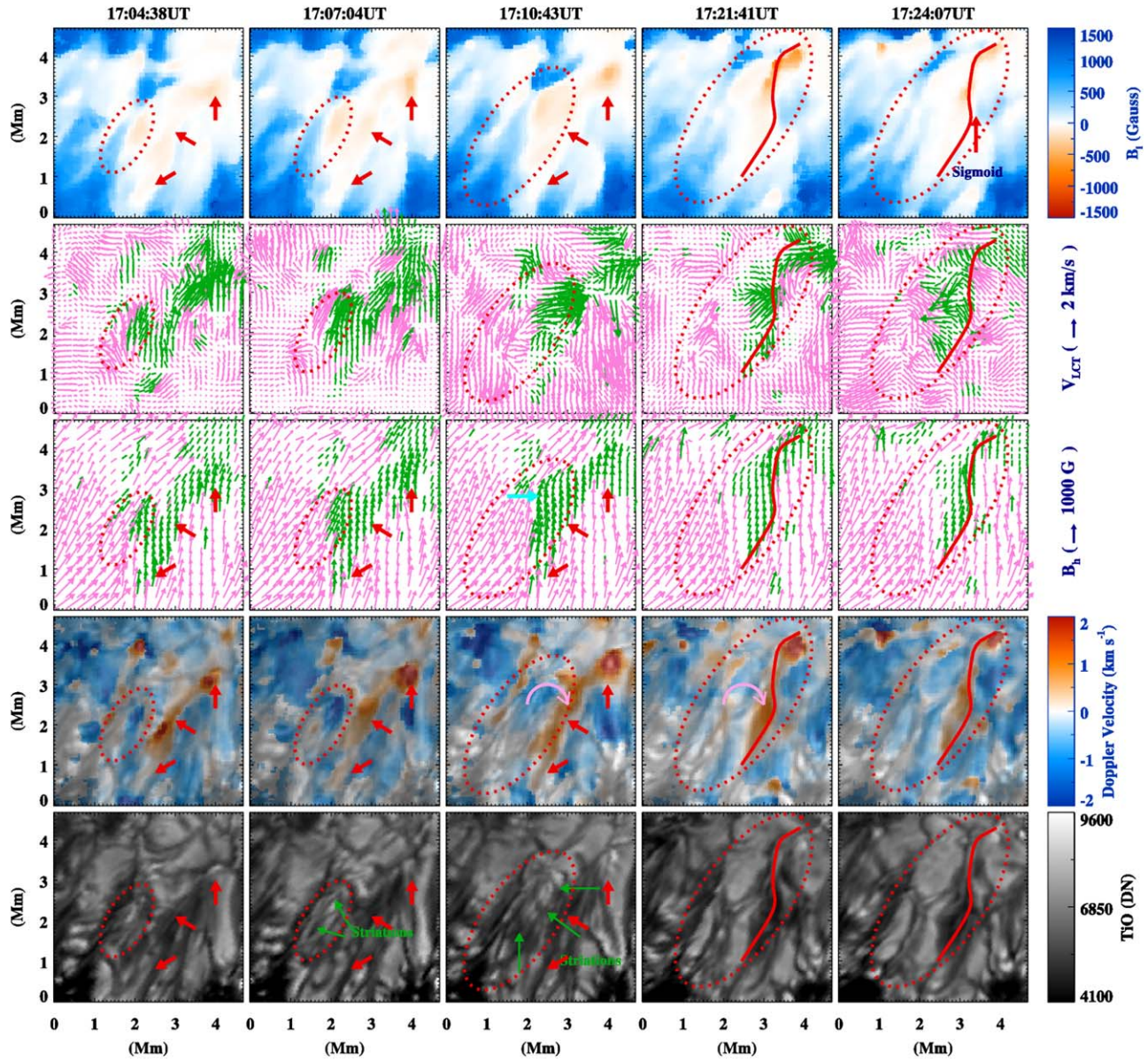


**Figure 3.** Magnetic and dynamic distributions in the ROI of the white square in Figure 1 during the appearance and submergence of the MMF. The LOS magnetic field $B_{\rm l}$, surface velocity $V_{\rm LCT}$, and horizontal magnetic field $B_{\rm h}$ are displayed in the upper three rows, respectively. The pink and green colors of the arrow in the panels of $V_{\rm LCT}$ and $B_{\rm h}$ indicate the locations with positive and negative $B_{\rm l}$ correspondingly. The composite image of the Doppler velocity and the TiO image is shown in the fourth row and the independent TiO intensity is shown in the bottom row. The MMF-relevant region at different time steps is outlined with the ovals in all panels. The annotations of other features are explained in the text.

distribution through the front part of the MMF, we find the MMF has a magnetic field strength of around 500 G and is dominated by the horizontal component when it collapses.

After time step 17:10:43 UT, the MMF-relevant region outlined by the oval does not present a coherent granule structure anymore. The twisted structure is then squashed into a limited region after 17:21:41 UT and forms a sigmoid-shaped flux tube, which submerges later. Rotation of the front part of the twisted structure after coalescence can be seen in the Doppler velocity, which is annotated with pink curved arrows. Opposite to the formed sigmoid structure in this limited region, the rest of the oval where the MMF passed through becomes more potential after 17:21:41 UT, i.e., the direction that the horizontal magnetic field pointed to is more perpendicular to the polarity inversion line.

The temporal evolution of vertical current density, local twist, and vertical current helicity are displayed in the three middle rows of Figure 4. The vector magnetic field and the TiO intensity image are shown in the top and bottom rows for reference. The white/black arrows overlaid on the images in the top four rows show the horizontal magnetic fields that correspond to positive and negative LOS magnetic fields, respectively. The MMF-relevant region is outlined by the dotted oval in each panel. The preexisting magnetic concentration is annotated with purple arrows for the first three time steps and the formed sigmoid structure is outlined with curved lines in all panels at time steps 17:21:41 UT and 17:24:07 UT. Beyond the striation features annotated at time steps 17:07:04 UT and 17:10:43 UT, a dark stripe that represents a penumbra-like filament structure is also labeled with green

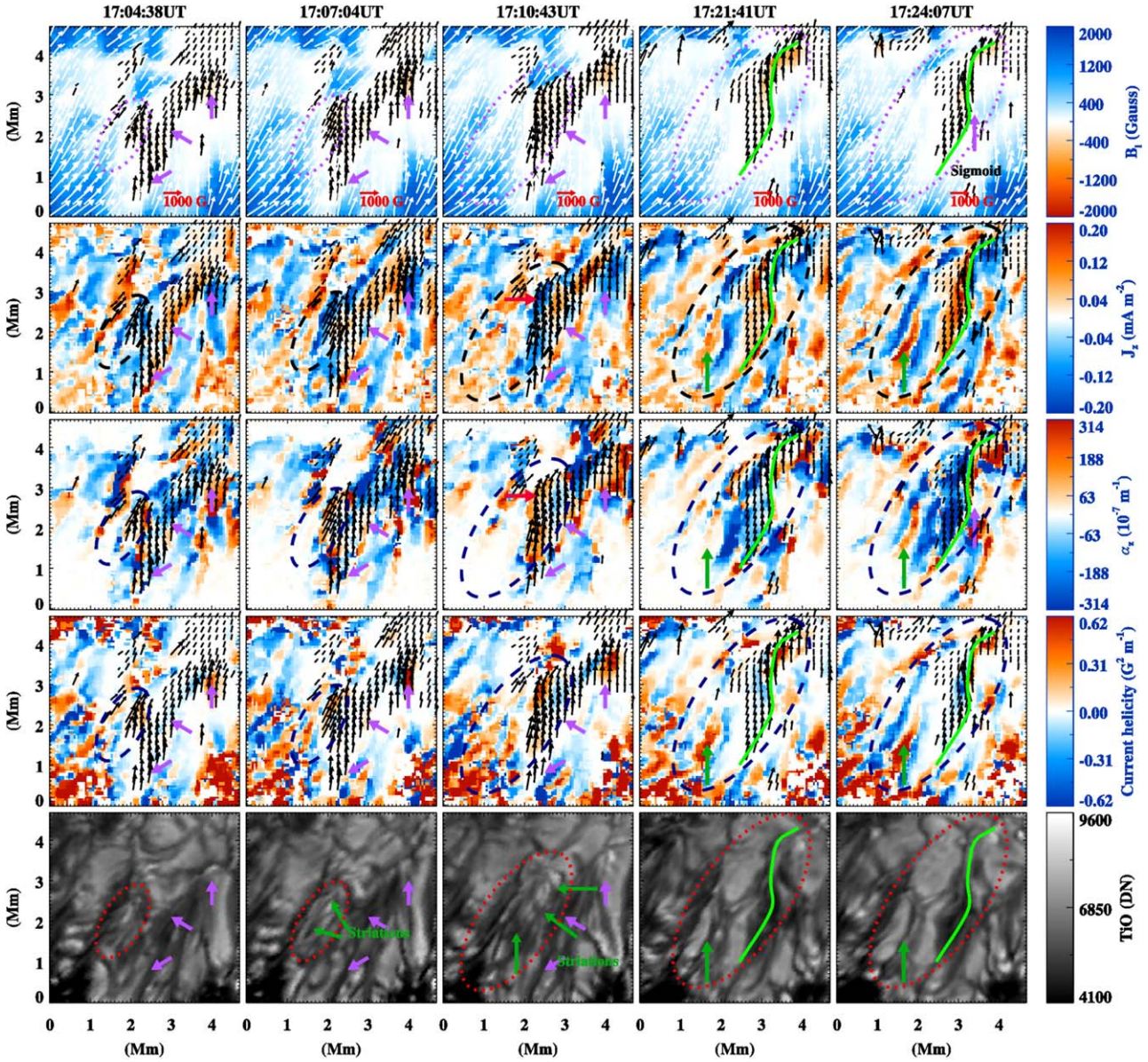


**Figure 4.** Calculated magnetic parameters, i.e., the vertical current density $J_z$, the local twist $\alpha$, and the vertical current helicity $H_z$ are displayed in the three middle rows. The $B_l$ and TiO intensities are shown in the top and bottom rows, respectively, for reference. The white/black arrows overlaid on the top four rows show the distribution of $B_h$ and the colors of white and black indicate locations of positive and negative $B_l$, respectively. The ovals and the other annotations have the same meanings as those displayed in Figure 3.

arrows at time steps 17:21:41 UT and 17:24:07 UT in the panels showing granular structure.

From the time step 17:04:38 UT–17:07:04 UT, the vertical current density inside the oval is relatively strong at the front part of the MMF and is dominated by negative values, while the local twist and vertical current helicity show a similar pattern but with the opposite sign. Elongated positive vertical current density is distributed at the back part of the preexisting magnetic concentration while negative density is distributed at the front part. The positive current density starts to coalesce with the MMF at time step 17:10:43 UT. By inspecting the distribution of magnetic parameters through the front part of the MMF (pointed by arrows in red in the third panels of the second and third rows), we find a larger twist number and vertical current density.

From the time step 17:21:41 UT–17:24:07 UT, the coalesced magnetic structure shows negative current density at the front and positive current density at the elongated back part with the sigmoidal shape. The local twist and the vertical current helicity also show a similar pattern but with opposite signs. Specifically, for the coalesced structure, the large helicity current density is limited to the sigmoidal region, while the $J_z$ and $\alpha$ have a more diffuse pattern. After the emergence of the MMF, the stripe patterns with positive and negative values adjacent to each other appear for all three parameters around the sunspot region, indicating a penumbra-like filament feature.

## 4. Striations and the Essence

The striations inside the elongated granular structures of the MMF are apparent at time steps 17:07:04 UT and 17:10:43 UT but with different orientations. Their associated magnetic features and velocity are displayed in Figures 5 and 6. To better display the granule and associated magnetic features, the

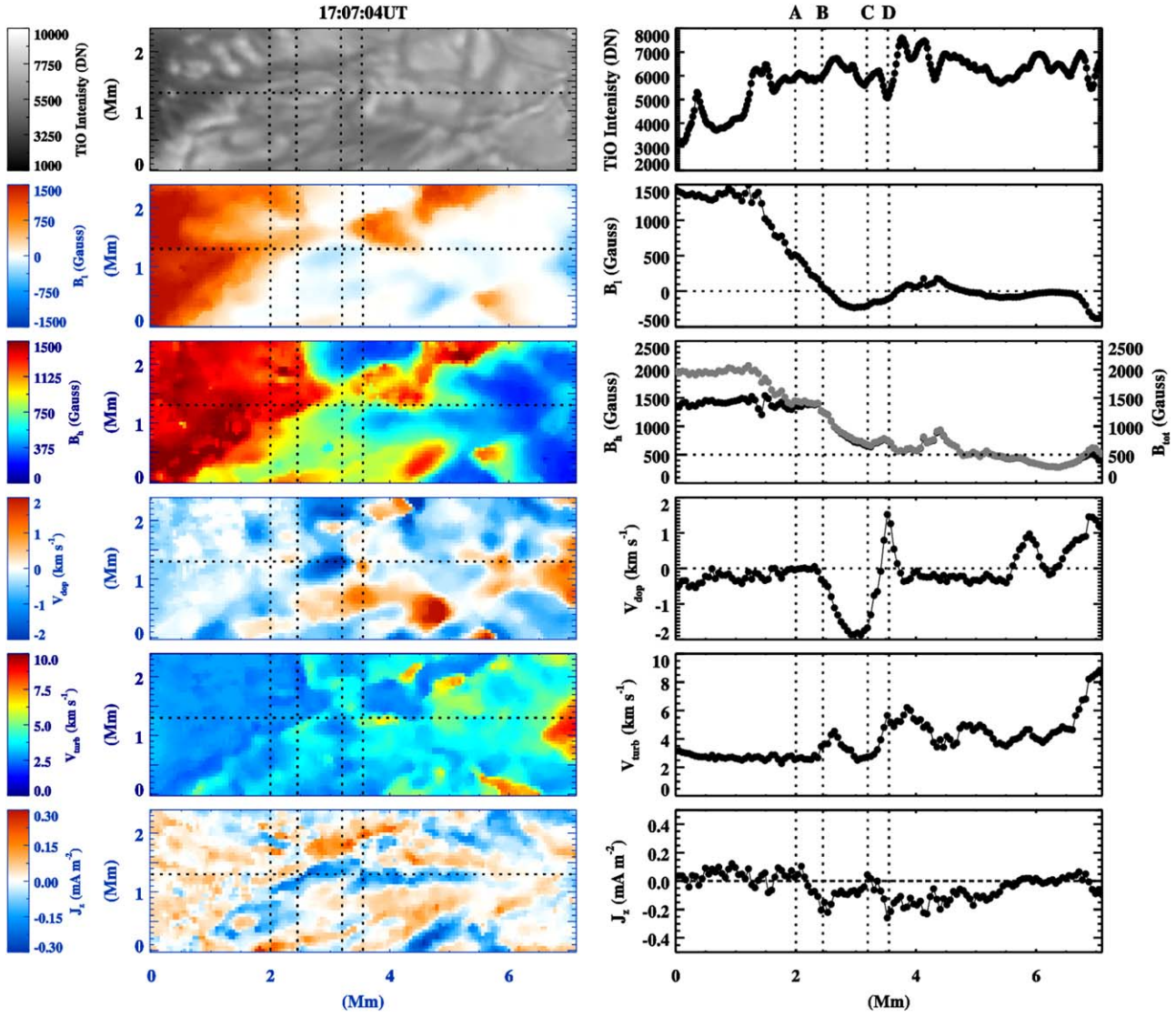


**Figure 5.** Demonstration of the magnetic and kinetics features of striations associated with the emerging flux. Left column: 2D images of a subregion in the ROI (rotated to present a horizontally elongated granule). Right column: line curves of different features that were sampled by the horizontal dotted lines in the left panels. The gray dotted line in the third panel of the right column shows the total magnetic field strength. The vertical lines in both columns, which are labeled with letters A, B, C, and D, respectively, are plotted to show the locations of different striations.

images in Figure 1 have been rotated and a subregion has been selected so that the major axis of the granule and associated magnetic features can be identified along a horizontal axis. The 2D distributions of associated parameters are shown in the left column and the related line profiles horizontally passing through the elongated granule are displayed in the right column. The vertical lines are selected manually to sample the striations with the leftmost line and rightmost line roughly outlining the horizontal boundaries of the elongated granules.

At both times, the total magnetic field of the MMF is greater than 500 G and is dominated by a horizontal magnetic field. The Doppler velocity shows blueshift at the region close to the pore and redshift farther away, which indicates an Evershed flow pattern. The turbulence velocity is large at places where the magnetic field is small (far away from the sunspot) and can reach the local maximum only in between the striations.

The properties of the striations, whose locations are annotated with letters A–D in Figure 5 and with A–E in Figure 6, vary one by one and may be intimately associated with the evolving magnetic field. Although the optical structure of the MMF shows significant differences at the two time steps, the magnetic and dynamic properties do not change much, only showing torsion and expansion to some extent. The above different evolution tendency between the optical structure and the magnetic structure might be related to their desynchrony during the dynamic process, i.e., the convection flow may modify the morphology of the granule while the magnetic structure would need more time to relax. Another possibility for the different tendencies might be related to the different spatial resolutions of the TiO image and the images of the magnetic parameters obtained from NIRIS. The latter one has a relatively lower spatial resolution, which could make it hard to distinguish the difference from temporal evolution as demonstrated in the TiO images.

## 5. Discussion and Conclusion

In this work, a detailed analysis has been carried out for the emergence and submergence of an MMF (Harvey & Harvey 1973)

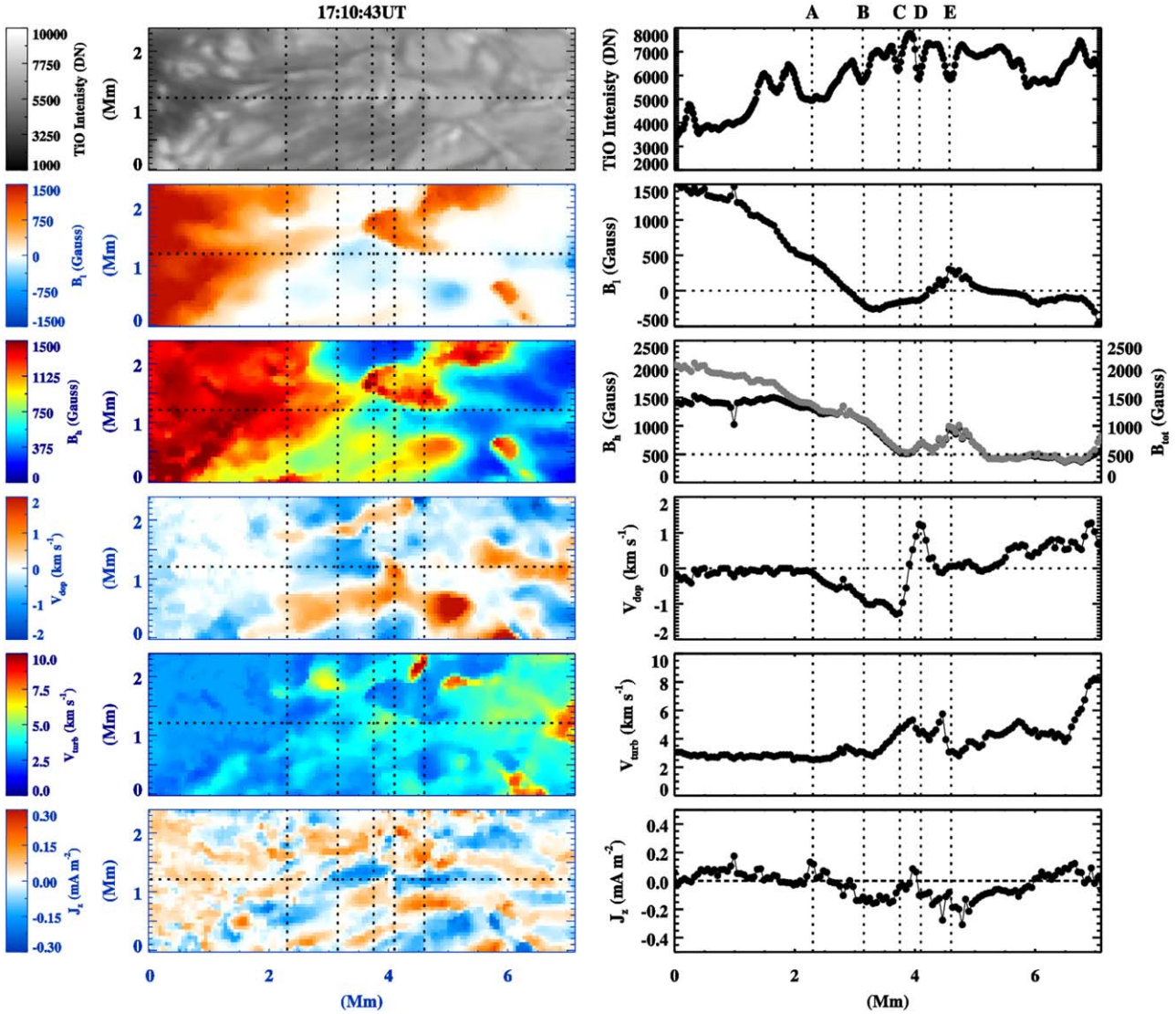


**Figure 6.** Same as in Figure 5 but at time step 17:10:43 UT. The vertical lines in both columns, which are labeled with letters A, B, C, D, and E, respectively, are plotted to show the locations of different striations.

around the pore at the periphery of a large sunspot. The magnetic field of the MMF is larger than 500 G and is dominated by a horizontal magnetic field. The extension of the granule associated with the MMF may be induced by the Evershed flow. The striations inside the granule have different properties but the overall magnetic and dynamic properties of the MMF remain stable. By coalescing with another magnetic concentration, the MMF turns into a sigmoid structure and finally submerges under the photosphere. After the emergence and submergence of the MMF, the ROI becomes more filamentary in the magnetic features, i.e., the vertical current density has elongated structures with positive and negative values adjacent to each other. However, we do not see the optical fibrils at the same time. This may indicate that the magnetic configuration may have existed before the appearance of the optical filamentary fibril around the pore (such as in Romano et al. 2013, 2014).

MMFs streaming away from a pore rather than the penumbra have been obtained in the specific case of spectropolarimetric observations from SUNRISE/IMaX (Kaithakkal et al. 2017), where different polarities of the MMFs have been identified with a spatial size of $0\farcs0545$ pixel$^{-1}$. The average speed of the MMFs is around 1.3 km s$^{-1}$, which is less than the speed in our case. Statistical analysis has also been carried out for an active region penumbra at different evolution stages (Zhang et al. 2003, 2007), where a U-loop model beneath the magnetic canopy is suggested for the evolution of the MMF. The average speed of the MMF in their study is less than 1 km s$^{-1}$ and mostly along the radial direction of the sunspot. In our case, the MMF is identified in the surroundings of a pore without a penumbra. It has a larger horizontal velocity of around 2 km s$^{-1}$ and also shows rotation during its movement outward along the radial direction. The horizontal expansion of the granule, which is associated with the magnetic flux emergence and with larger velocity, has been found. Shen et al. (2022) found granular-scale emergence around 2–3 km s$^{-1}$ in between the emerging regions but this was associated with eruptive events; Lim et al. (2011) found flux emergence stretching out at a speed of over 4 km s$^{-1}$ from the penumbra filament and subsequent flux cancellation.

MMFs associated with filamentary fibril formation around a protospot have rarely been observed. During the penumbra formation at one side of the pore, MMFs have been observed

on the other side of the pore moving toward the protospot (Schlichenmaier et al. 2010a, 2010b). Two elongated microfilaments that connect the penumbra and the MMF have been observed in the chromosphere during the period of the MMF stretching out from the penumbra, with a lifetime of 3 hr and 0.1 hr, respectively (Li & Zhang 2013). Observations also show the penumbra forms at the expense of the umbra (Jurčák et al. 2017), which is difficult to identify in our study due to the intermittent observations of the Stokes profiles.

Different categories of MMFs have been found around the protospot (Kaithakkal et al. 2017) or in the penumbra of decaying active regions (Zhang et al. 1992), with one kind showing a single polarity, either the same or the opposite as the center sunspot, and another kind showing bipolar field, although some high-resolution observations suggest that the single-polarity MMF is actually comprised of both polarities but on a small scale (Hagenaar & Shine 2005). In theoretical works, the MMF could be induced by the kink instability under the environment of shear flows (Ryutova et al. 1998) or through the "downward pumping" of the magnetic field, which forms the filamentary structures that are the basic components of the penumbra (Thomas et al. 2002). In the latter model, three types of MMFs are suggested. The type I MMF is related to the pop-up of the submerged horizontal flux tube with an outward velocity of 0.5–1 km $s^{-1}$. The type II MMF is associated with the decaying of the active region while a type III MMF may occasionally happen when the pumping mechanism raises the submerged magnetic flux tube entirely, and the outward speed reaches 2–3 km $s^{-1}$. Our observations are most similar to the type III MMF but with a more complex topology than the buoyantly raised part of the horizontal field in the penumbra region.

To understand the dynamics and the fine dark core of the penumbra filament, a "screw pinch" configuration is used to describe the stability of a cylindrical magnetic flux tube in Ryutova et al. (2008). A safety factor $q = \frac{2\pi RB_z}{LB_\phi}$ is defined for interpreting the screw pinch instability, where $R$ is the radius of the magnetic flux tube and $L$ is the length. $B_z$ is the axial magnetic field and $B_\phi$ is the azimuthal field. By assuming the length of the magnetic flux tube to be three times its radius, and the axial magnetic field and the azimuthal field to be the horizontal magnetic field and LOS magnetic field, respectively, the screw pinch instability of the magnetic flux tube is also estimated for the MMF in our case. The calculated "safety factor" is less than 1, indicating the magnetic flux tube is "under safe" according to Ryutova et al. (2008). Hence, a convection-dominated rotation of the magnetic flux tube is suggested for the phenomenon investigated here.

Dark striations inside penumbra filaments have been identified with high-resolution observations of the Swedish 1 m Solar Telescope (Scharmer et al. 2002) and Hinode (Ichimoto et al. 2007). Such dark striations are considered to be evidence of the convection flow in the penumbra region (Zakharov et al. 2008; Bharti et al. 2010) or associated with sideway swaying of the central upflow in the penumbra filament (Bharti et al. 2012). In the MMF studied in the present work, dark striations are also identified during the rotation of the MMF. The striations show different properties of the dynamic feature, but convective downflow at these locations cannot be identified, as they could be hidden in the overall rotation of the MMF. As the MMF evolution is much more dynamic than that of the relatively stable penumbra filament, the oscillation found in previous works for the dark striation is not analyzed either.

In conclusion, the high spatial resolution of the instruments enables us to observe the coupling between convection and the emergence of a magnetic field. With the Daniel K. Inouye Solar Telescope (Rast et al. 2021), we should be able to further understand how the coupling is effectively achieved.

## Acknowledgments

We thank Dr. Zhi Xu for the fruitful discussion. We thank Dr. Sarah Gibson for reading and polishing the paper. J.Z. acknowledges the support by the Strategic Priority Research Program of the Chinese Academy of Sciences (grant No. XDB0560302), the National Key R&D Program of China (grant No. 2022YFF0503001), and the Youth Innovation Promotion Association CAS (grant No. 2023333). This work is also supported by the National Natural Science Foundations of China (grant Nos. 12233012, 11973012, 12333009, and 11820101002). We gratefully acknowledge the use of data from the Goode Solar Telescope (GST) of the Big Bear Solar Observatory (BBSO). BBSO operation is supported by US NSF AGS-2309939 and AGS-1821294 grants and the New Jersey Institute of Technology. GST operation is partly supported by the Korea Astronomy and Space Science Institute and the Seoul National University. X.Y. acknowledges support from US NSF AST-2108235.

## ORCID iDs

Jie Zhao https://orcid.org/0000-0003-3160-4379
Fu Yu https://orcid.org/0000-0002-1713-2160
Xiaoshuai Zhu https://orcid.org/0000-0002-1682-1714
Xu Yang https://orcid.org/0000-0002-3238-0779
Jiangtao Su https://orcid.org/0000-0002-5152-7318
Brigitte Schmieder https://orcid.org/0000-0003-3364-9183
Hui Li https://orcid.org/0000-0003-1078-3021
Wenda Cao https://orcid.org/0000-0003-2427-6047

## References

Ahn, K., & Cao, W. 2019, in ASP Conf. Ser. 526, Solar Polarization Workshop 8, ed. L. Belluzzi et al. (San Francisco, CA: ASP), 317
Ahn, K., Cao, W., Shumko, S., & Chae, J. 2016, AAS/SPD Meeting, 47, 2.07
Bharti, L., Cameron, R. H., Rempel, M., Hirzberger, J., & Solanki, S. K. 2012, ApJ, 752, 128
Bharti, L., Solanki, S. K., & Hirzberger, J. 2010, ApJL, 722, L194
Cao, W., Goode, P. R., Ahn, K., et al. 2012, in ASP Conf. Ser. 463, Second ATST-EAST Meeting: Magnetic Fields from the Photosphere to the Corona, ed. T. R. Rimmele et al. (San Francisco, CA: ASP), 291
Cao, W., Gorceix, N., Coulter, R., et al. 2010, AN, 331, 636
Criscuoli, S., Del Moro, D., Giannattasio, F., et al. 2012, A&A, 546, A26
Deng, N., Choudhary, D. P., Tritschler, A., et al. 2007, ApJ, 671, 1013
Evershed, J. 1909, MNRAS, 69, 454
Hagenaar, H. J., & Shine, R. A. 2005, ApJ, 635, 659
Harvey, K., & Harvey, J. 1973, SoPh, 28, 61
Ichimoto, K., Suematsu, Y., Tsuneta, S., et al. 2007, Sci, 318, 1597
Jurčák, J., Bello González, N., Schlichenmaier, R., & Rezaei, R. 2017, A&A, 597, A60
Kaithakkal, A. J., Riethmüller, T. L., Solanki, S. K., et al. 2017, ApJS, 229, 13
Kubo, M., Shimizu, T., & Lites, B. W. 2003, ApJ, 595, 465
Leka, K. D., Barnes, G., Crouch, A. D., et al. 2009, SoPh, 260, 83
Li, K.-J., Shen, Y.-D., Yang, L.-H., & Jiang, Y.-C. 2010, ChA&A, 34, 142
Li, Q., Deng, N., Jing, J., Liu, C., & Wang, H. 2019, ApJ, 876, 129
Li, X., Yang, Z., & Zhang, H. 2015, ApJ, 807, 160
Li, X., & Zhang, H. 2013, ApJ, 771, 22
Lim, E.-K., Yurchyshyn, V., Abramenko, V., et al. 2011, ApJ, 740, 82
Lim, E.-K., Yurchyshyn, V., & Goode, P. 2012, ApJ, 753, 89
Martínez Pillet, V. 2002, AN, 323, 342

Peng, Y., Xue, Z., Qu, Z., et al. 2024, ApJ, 960, 95
Rast, M. P., Bello González, N., Bellot Rubio, L., et al. 2021, SoPh, 296, 70
Rezaei, R., Bello González, N., & Schlichenmaier, R. 2012, A&A, 537, A19
Romano, P., Frasca, D., Guglielmino, S. L., et al. 2013, ApJL, 771, L3
Romano, P., Guglielmino, S. L., Cristaldi, A., et al. 2014, ApJ, 784, 10
Ryutova, M., Berger, T., & Title, A. 2008, ApJ, 676, 1356
Ryutova, M., Shine, R., Title, A., & Sakai, J. I. 1998, ApJ, 492, 402
Sainz Dalda, A., & Bellot Rubio, L. R. 2008, A&A, 481, L21
Sainz Dalda, A., & Martínez Pillet, V. 2005, ApJ, 632, 1176
Scharmer, G. B., Gudiksen, B. V., Kiselman, D., Löfdahl, M. G., & Rouppe van der Voort, L. H. M. 2002, Natur, 420, 151
Schlichenmaier, R. 2002, AN, 323, 303
Schlichenmaier, R., Bello González, N., Rezaei, R., & Waldmann, T. A. 2010a, AN, 331, 563
Schlichenmaier, R., Rezaei, R., Bello González, N., & Waldmann, T. A. 2010b, A&A, 512, L1
Sheeley, N. R. J. 1969, SoPh, 9, 347
Shen, J., Xu, Z., Li, J., & Ji, H. 2022, ApJ, 925, 46
Su, J. T., Sakurai, T., Suematsu, Y., Hagino, M., & Liu, Y. 2009, ApJL, 697, L103
Thomas, J. H., Weiss, N. O., Tobias, S. M., & Brummell, N. H. 2002, Natur, 420, 390
Wang, H., Liu, C., Ahn, K., et al. 2017, NatAs, 1, 0085
Weiss, N. O., Thomas, J. H., Brummell, N. H., & Tobias, S. M. 2004, ApJ, 600, 1073
Wöger, F., von der Lühe, O., & Reardon, K. 2008, A&A, 488, 375
Yang, X., Cao, W., & Yurchyshyn, V. 2022, ApJS, 262, 55
Yang, X., Yurchyshyn, V., Ahn, K., Penn, M., & Cao, W. 2019, ApJ, 886, 64
Yurchyshyn, V. B., Wang, H., & Goode, P. R. 2001, ApJ, 550, 470
Zakharov, V., Hirzberger, J., Riethmüller, T. L., Solanki, S. K., & Kobel, P. 2008, A&A, 488, L17
Zhang, H., Ai, G., Wang, H., Zirin, H., & Patterson, A. 1992, SoPh, 140, 307
Zhang, J., Solanki, S. K., & Wang, J. 2003, A&A, 399, 755
Zhang, J., Solanki, S. K., Woch, J., & Wang, J. 2007, A&A, 471, 1035
Zhao, J., Su, J., Yang, X., et al. 2022, ApJ, 932, 95
Zuccarello, F., Romano, P., Guglielmino, S. L., et al. 2009, A&A, 500, L5